Mater Renew Sustain Energy (2015) 4:2
DOI 10.1007/s40243-015-0042-0

ORIGINAL PAPER

Copper nanoparticles stabilized by reduced graphene oxide for CO_2 reduction reaction

Diego C. B. Alves · Rafael Silva · Damien Voiry · Tewodros Asefa · Manish Chhowalla

Received: 10 October 2014 / Accepted: 16 January 2015

Abstract Carbon dioxide (CO_2) is one of the main gases produced by human activity and is responsible for the green house effect. Numerous routes for CO_2 capture and reduction are currently under investigation. Another approach to mitigate the CO_2 content in the atmosphere is to convert it into useful species such as hydrocarbon molecules that can be used for fuel. In this view, copper is one of the most interesting catalyst materials for CO_2 reduction due to its remarkable ability to generate hydrocarbon fuels. However, its utilization as an effective catalyst for CO_2 reduction is hampered by its oxidation and relatively high voltages. We have fabricated hybrid materials for CO_2 reduction by combining the activity of copper and the conductivity of reduced graphene oxide (rGO). Cu nanoparticles (CuNPs) deposited on rGO have demonstrated higher current density and lower overpotential compared to other copper-based electrodes that we have tested. The CuNPs on rGO also exhibit better stability, preserving their catalytic activity without degradation for several hours.

Keywords CO_2 reduction · Synthetic photosynthesis · Reduced graphene oxide · Copper nanoparticles · Electrocatalysis

Introduction

The increasing demand for renewable energy has been motivating researchers around the world to pursue the development of new technologies. Various methods and devices to generate sustainable forms of energy that are efficient and affordable have been reported [1–4]. In addition to clean energy, the high amount of CO_2 emitted in the atmosphere must also be mitigated [5, 6]. The use of CO_2 as a feedstock to generate fuels is intriguing and inspired by photosynthesis [7]. The consumption of CO_2 from the atmosphere via its conversion to fuel could provide new sources of energy. In this view, electrochemical reduction of CO_2 appears promising since it can lead to formation of methane, ethylene, methanol, formate, carbon monoxide, formic acid and other compounds that can be potentially used as fuels [8–10]. The applicability of the CO_2 reduction process is currently limited by the high overpotentials even when using noble metal catalysts as active electrodes [11].

Different materials have been investigated as catalysts for CO_2 reduction. Some candidates such as Hg, In and Cd have shown high current efficiency associated with high hydrogen overvoltage but remain poor choice for CO_2 reduction catalysts because of their low selectivity in

Electronic supplementary material The online version of this article (doi:10.1007/s40243-015-0042-0) contains supplementary material, which is available to authorized users.

D. C. B. Alves · D. Voiry · M. Chhowalla
Materials Science and Engineering, Rutgers University, 607 Taylor Road, Piscataway, NJ 08854, USA

D. C. B. Alves (✉)
Departamento de Física, Universidade Federal de Minas Gerais, Belo Horizonte, MG 31270-901, Brazil
e-mail: diego.c.b.physicist@gmail.com; dbarbosa@fisica.ufmg.br

R. Silva · T. Asefa
Department of Chemistry and Chemical Biology, Rutgers University, 610 Taylor Road, Piscataway, NJ 08854, USA

T. Asefa
Department of Chemical and Biochemical Engineering, Rutgers University, 98 Brett Road, Piscataway, NJ 08854, USA

Published online: 06 February 2015

producing the desired products [12]. On the other hand, materials such as Pt, Ni, Fe and Ti favor hydrogen evolution reaction (HER) in aqueous media and also possess high affinity to CO, leading to rapid reduction of catalytic activity [13]. Copper is the most promising catalyst for CO_2 reduction reaction because it enables the production of hydrocarbons at significant current densities, exhibits good selectivity, and has low surface affinity to CO [14]. Theoretical studies have shown that CO acts as an important precursor for hydrocarbon synthesis, which progresses in successive hydrogenation/reduction reactions [15] leading to the 16 products identified during CO_2 reduction on copper [9]. Despite its rich electrochemistry, Cu suffers from high overpotentials compared to potentials of standard catalysts for hydrocarbon production (0.17 V vs. RHE) [9, 16]. Challenges associated with high overpotential and low electrochemical stability must be overcome if copper is to be seriously considered as a practical catalyst for CO_2 reduction reaction [16]. It has been demonstrated that the oxide passivation layer on a Cu film can reduce the overpotential for the CO_2 reduction reaction as well enhance the stability [17]. Although passivated Cu films are more robust catalysts, it leads to a reduction of the current density due to the copper oxide layer. Cu nanoparticles (NPs) could be beneficial in facilitating the CO_2 reduction reaction but their instability caused by combined effects of aggregation and rapid deactivation of the catalytic surface via oxidation has limited their consideration. One strategy recently proposed to overcome the stability issues was to use Au_2Cu NPs that are less prone to oxidation instead Cu NPs for CO_2 reduction [18]. However, Au is expensive and also known to be a good catalyst for HER that can disrupt the production of hydrocarbons [19]. In the present work, we demonstrate that reduced graphene oxide decorated with copper NPs (CuNPs on rGO) is a promising catalyst system for CO_2 reduction that exhibits remarkable stability in a medium with low proton availability. CuNPs on rGO electrodes exhibit lower overpotential for CO_2 reduction reaction and show a strong increase in the current density. To assess the stability of the catalysts, we have tested CuNPs on rGO for several hours and found limited decrease in the current density and negligible change in the overpotential.

Graphene oxide (GO) has been investigated for a broad range of applications in electronics [20], biology [21], energy storage [22, 23], and more recently in catalysis [24–26]. GO consists of atomically thin sheets with lateral dimensions of a few micrometers and thickness of less than 1 nm. GO is composed of sp^2 and sp^3 carbon bonds as well as oxygen functional groups such as hydroxyls and carbonyls [27, 28]. Its chemically heterogeneous properties can be tuned to some extent by varying the oxygen content through reduction and offer a remarkable platform for performing novel chemistry [29, 30]. The partial removal of oxygen functional groups leads to an enhancement in the π conjugation so that the semi-metallicity of graphene is partially restored and its conductivity increases by several orders of magnitude compared to as-prepared GO [31, 32]. Recently, it has been reported that reduced graphene oxide (rGO) works synergistically with catalyst particles to enhance their stability and performance [33–36].

Experimental

The synthesis was performed in two steps as shown in Scheme 1. First, an aqueous solution of GO was prepared at a concentration of 1.5 mg/mL and this solution was mixed with 9 mg of $CuSO_4$ (copper II sulfate). NaOH was then added and the mixture was vigorously stirred at 70 °C for 5 min. At this step of the synthesis, the color of the solution changed to dark grey. Then, 625 μL of hydrazine was quickly added to the mixture and stirred for additional 40 min. Upon the addition of hydrazine, the color turned dark violet. The mixture was further washed several times with EtOH by centrifugation (10 min at 30 k rpm).

Graphene oxide synthesis

Graphene oxide (GO) was prepared chemically via modified Hummer's method [37]. The graphite powder (Branwell Graphite Inc.) with size of >425 μm was chemically oxidized, exfoliated, and purified by repeated centrifugation.

Copper nanoparticles passivated with polyallylamine

Cu nanoparticles are prepared following the procedure proposed by Wang and Asefa [38], using polyallylamine as passivating agent. In the present case, 220 μL polyallylamine (Sigma-Aldrich) was completely dissolved in distilled water under vigorous stirring at 70 °C. Then, 9 mg of copper sulfate (Sigma-Aldrich) was added followed by

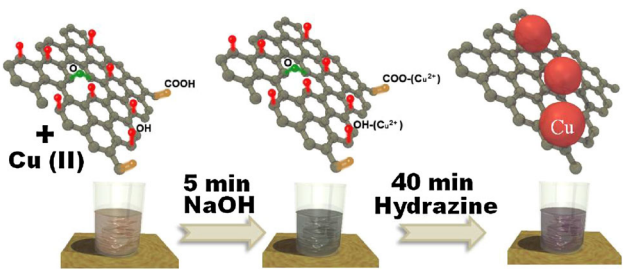

Scheme 1 Schematic representation of the synthesis method consisting of mixing GO with copper(II) and NaOH first. Hydrazine was then added and the mixture was stirred for 40 min. The final material corresponds to rGO nanosheets decorated with Cu NPs

700 μL of NaOH 0.5 M. After 5 min, ~60 μL of hydrazine was poured in the mixture. The solution color changed from an initial blue color to brown and 40 min later the solution color became red.

Copper thin film

A thin film of copper was formed by electrochemical deposition using a solution with 19 mg of Cu(I) in 10 mL acetonitrile. The copper was deposited on a glassy carbon electrode with 3 mm diameter. The deposition was carried out using a constant current of 10 μA for 10 min giving approximately 4 μg of deposited copper. Considering the density of bulk copper and the diameter of the glassy carbon, the thickness of the copper film is estimated to be around 70 nm.

Characterization

X-ray photoelectron spectroscopy (XPS) measurements were performed with a Thermo Scientific K-Alpha spectrometer. All spectra were taken using an Al Kα microfocused monochromatized source (1,486.6 eV) with a resolution of 0.6 eV. Raman spectra were obtained using a Renishaw 1,000 system operating at 514 nm. The UV–vis absorption spectra were measured with a Lambda 950 spectrophotometer (PerkinElmer). Transmission electron microscope (TEM) images of the samples were obtained with a Topcon 002B TEM that was working at an acceleration voltage of 200 kV.

Electrochemical measurements

The measurements (VersaStat 3 potentiostat from Princeton Applied Research) consist of linear sweep voltammetry (LSV) and were performed in two distinct environments (Argon and CO_2) using acetonitrile (10 mL) and tetra-*n*-butylammonium hexafluorophospate (NBu_4PF_6) (387 mg, Alfa Aesar) as electrolyte. The electrolyte solution was first degassed using argon for 30 min. Under this condition, no reduction reaction is expected. The same procedure was repeated under CO_2 to saturate the solution prior the measurements.

All materials were deposited by drop casting on glassy carbon electrode (CH Instruments, Inc.) and the current of the voltammograms is normalized by the geometric area ($\sim 7 \times 10^{-2}$ cm^2) of the glassy carbon. An Ag/Ag^+ (0.1 m) electrode in acetonitrile and a platinum wire were used as reference and counter electrode, respectively. The reference electrode was calibrated using the well-known reduction oxidation signals of ferrocene (FCN) (Figure S1). Potentials in the voltammograms are corrected to NHE.

Results and discussion

RGO decorated with CuNPs was synthesized by co-reduction of copper(II) and GO using hydrazine solution as reducing agent. Briefly, copper(II) sulfate (9 mg) and GO (3 mg) were dispersed in 10 mL of 0.5 M NaOH at 70 °C under vigorous stirring. In basic solution, copper(II) cations remain in close contact with the negatively charged oxygen functional groups of GO. 625 μL of 80 % hydrazine solution was then poured into the mixture to reduce copper(II) and the GO nanosheets (see Methods for details). The addition of hydrazine results in a significant change in the color of the solution, becoming intensely reddish due to surface plasmon resonance (SPR) effect of metallic copper nanoparticles. This effect causes strong absorption around 580–600 nm [39]. As a result of the co-reduction process, conductive rGO is obtained along with metallic copper nanoparticles formed via reduction of Cu(II) as shown in Scheme 1. It is worth noting that no additional passivating agents, such organic molecules or polymers, were used to stabilize the as-prepared copper particles. TEM images of the composite indicate that the CuNPs are uniformly distributed on the basal plane of the reduced graphene oxide and it was also observed that some nanoparticles were partially wrapped by the rGO sheets (Fig. 1a). TEM observations suggest that rGO acts as a stabilizing support for the 20–40 nm Cu nanoparticles by immobilizing and preventing their aggregation into larger particles (inset Fig. 1a).

Figure 1b presents FTIR spectra of the CuNPs on rGO and bare rGO films reduced by hydrazine. Clear differences between the two spectra can be observed. First, the rGO spectrum reveals the absence of oxygen functionalized groups, suggesting a strong reduction [40]. In contrast, the intense bands between 800 and 1,330 cm^{-1} in the CuNPs/rGO spectrum correspond to stretching vibrations (mainly from epoxy and ketone groups), which suggests that decoration with CuNPs inhibits a more severe reduction of GO. However, contributions in the 1,500–1,600 cm^{-1} range are typically not related to oxygen groups, and can be assigned to the asymmetric stretch of sp_2-hybridized C=C within the rGO basal plane [41]. The presence of residual hydroxyl has been demonstrated to be beneficial in catalysis through enhancement of electrochemical stability and catalytic activity [41, 42]. In addition, hydroxyl groups that remain on rGO nanosheets decrease the interface energy between rGO and copper, leading to stabilization of CuNPs.

To further investigate the structure of copper-decorated rGO, X-ray photoelectron spectroscopy (XPS) was performed. From the XPS survey spectrum of CuNPs/rGO hybrid material shown in Fig. 2, it is possible to identify signals from oxygen, carbon and copper. The upper left

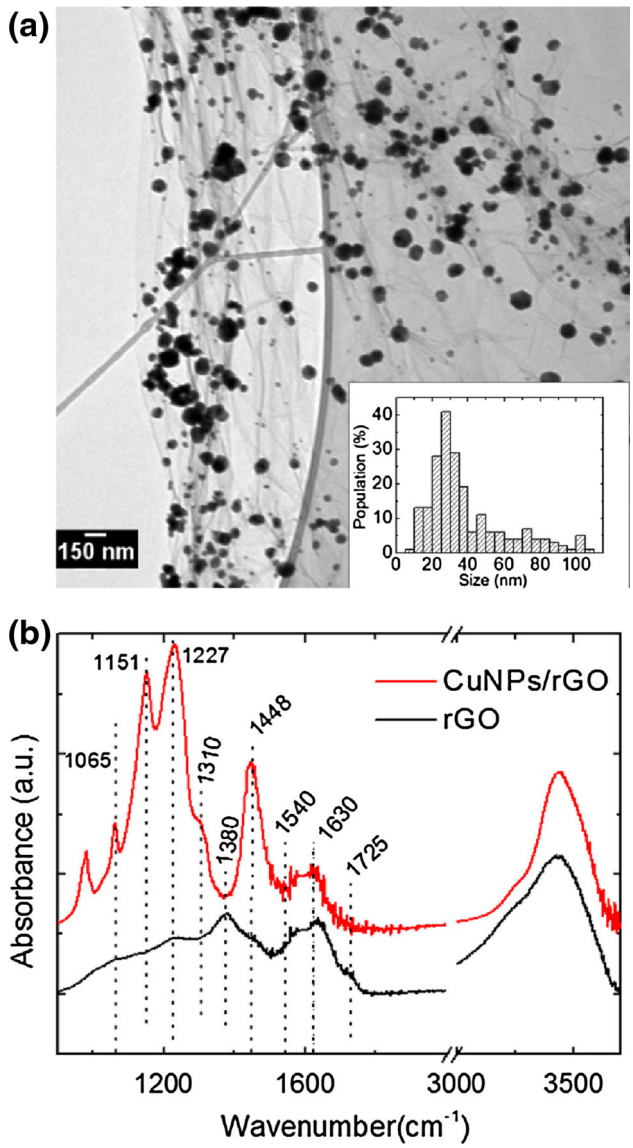

Fig. 1 TEM image and FTIR of CuNPs on rGO prepared by hydrazine reduction: **a** TEM image showing the dispersion of nanoparticles on rGO. The size distribution histogram indicates an average particle size of about 30 nm. **b** FTIR spectra of bare rGO and CuNPs on rGO. The oxygen peaks are virtually absent in bare rGO while they are present in Cu NP decorated rGO and are presumably helping the stabilization of the Cu NPs

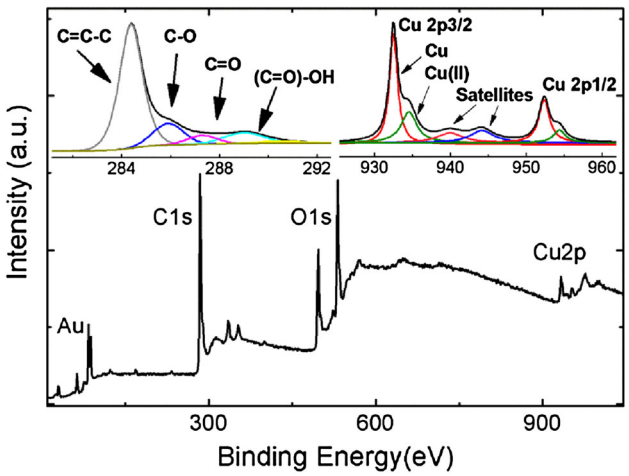

Fig. 2 XPS survey spectrum of CuNPs on rGO. High-resolution spectra from the C1s and Cu2p regions can be deconvoluted with different components from various chemical bonds, as indicated by the fits in the *upper portion* of the figure

inset shows the high-resolution signal of the C1s region from rGO with C–C/C=C, C–OH/C–O, C=O and C=O–OH peaks at 284.4, 286, 287.3, 289 and the satellite peak at 290.6 eV. After hydrazine treatment, the carbon/oxygen ratio in the CuNPs on rGO sample increased from 2.1 up to 7.3. This value is in good agreement with those previously reported for mildly reduced GO [43, 44]. On the other hand, peaks from Cu $2p_{3/2}$ and $2p_{1/2}$ can be identified at 932.5 and 952.4 eV, respectively. The fitting of the Cu peaks reveals a main signal at 932.5 eV that can be attributed to the zero-valence states of Cu and smaller peaks at 934.4 eV that are due to the presence of Cu(II) [17]. The latter indicates partial oxidation of the Cu nanoparticle surface in the form of CuO. We believe that the CuO shell is formed during exposure to air after the synthesis since the presence of hydrazine during nanoparticle synthesis is likely to prevent copper from being oxidized. It is also possible to verify the presence of two Cu satellites bands at 940 and 943.9 eV. Moreover, the presence of copper in zero-valence state is also confirmed by our UV–Vis spectroscopy results (see Supplementary Information, Figure S2) that show an intense absorption band at around 600 nm attributed to the surface plasmon resonance effect (SPR) in metallic copper NPs as previously reported [45–47]. This peak is not observed in the UV–Vis spectrum of the bare rGO, Figure S2. The SPR band was also observed at 560 nm for CuNPs prepared using polyallylamine as capping agent. The shift in position of copper SPR band between CuNPs prepared with polyallylamine and CuNPs on rGO can be attributed to differences in the size of the nanoparticles. That is, our TEM image analyses show that the Cu NPs prepared using polyallylamine are significantly smaller in size than the CuNPs on rGO (Figure S3).

CO_2 reduction reaction

To gain insight into the catalytic activity of copper nanoparticles on rGO, cyclic voltammetry was performed in argon (Ar)- and CO_2-saturated electrolyte solutions (Fig. 3). It has been recently reported that the selectivity toward the chemical species is highly dependent on the morphology of polycrystalline copper [48]. To limit the number of products from the CO_2 reduction, all the measurements reported here have been performed in the

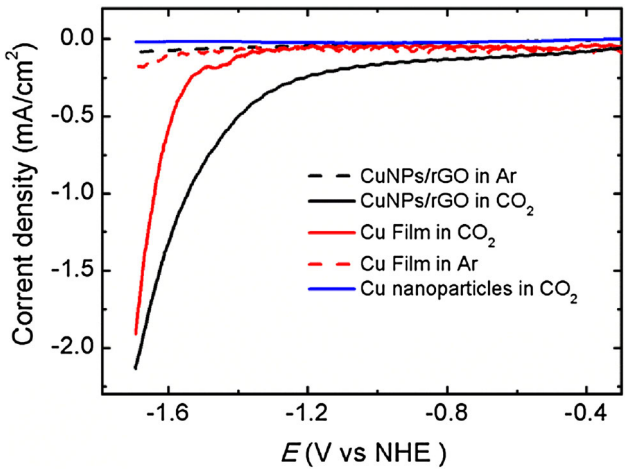

Fig. 3 Linear sweep voltammetry (LSV) of CuNPs/rGO, Cu thin film and polymer passivated CuNPs under Argon- and CO_2-saturated solutions. The Cu NPs on rGO electrodes exhibit lower overpotential and higher current density compared to other forms of copper tested in this study

absence of water. Specifically, the experiments were performed in acetonitrile using Tetra-n-butylammonium hexafluorophosphate (NBu_4PF_6, 0.1 M) electrolyte. Acetonitrile was chosen because it can dissolve approximately eightfold more CO_2 than water [49], and also because it is a low hydrogen availability medium so that the contribution from HER on the cathodic current can be largely disregarded. In addition, the mechanism for CO_2 reduction in low hydrogen availability medium is well known. Only three species can be obtained: carbon monoxide (CO), carbonate (CO_3^{2-}) or oxalate ($C_2O_4^{2-}$) involve 2 electrons each (Equation I and II). Oxalate formation requires C–C coupling which is known to occur at higher overpotentials (>0.9 V vs. RHE) [9, 10]. Experiments in DMF with low proton content similar to acetonitrile have demonstrated that oxalate and CO are the two main products of the reaction and only traces of HCO_2^- have been detected [50].

$$2CO_2 + 2e^- \rightarrow C_2O_4^{2-} \quad (1)$$

$$2CO_2 + 2e^- \rightarrow CO + CO_3^{2-} \quad (2)$$

The activity of the electrodes can be easily tested by comparing the cathodic current in solution saturated with CO_2 with the cathodic current in solution saturated with Ar. It is worth noting that the potentials to reduce Cu (II) to Cu (I) and Cu(I) to Cu metal in organic medium are approximately −0.3 and −0.6 V vs. NHE, respectively [51]. Thus, at the range of negative potentials used here for CO_2 reduction, the reduction of the copper oxide shell is thermodynamically favored and the nanoparticles are most likely being reduced to copper metal [48]. From Fig. 3, the CO_2 reduction is clearly demonstrated by the high cathodic

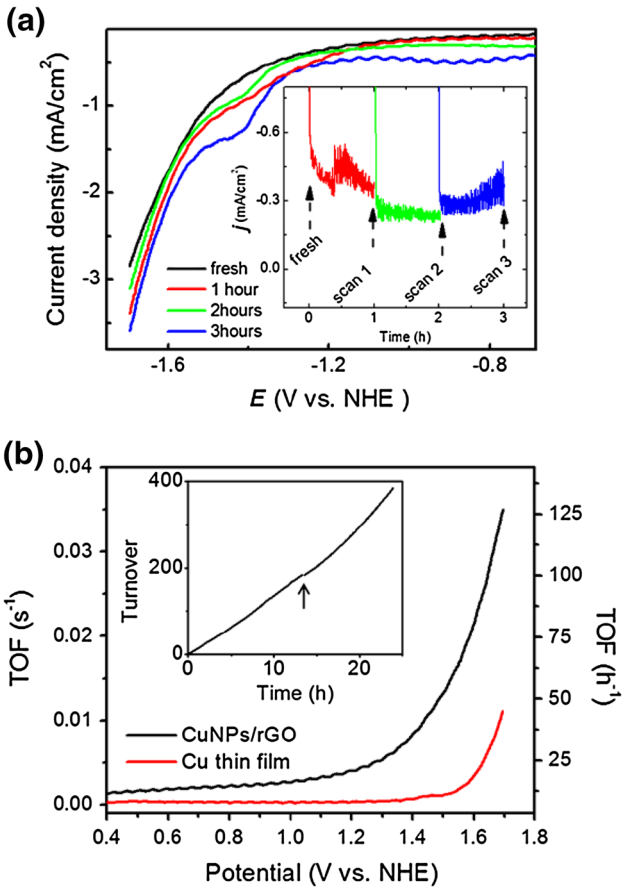

Fig. 4 **a** Linear sweep voltammetry (LSV) curves for CuNPs on rGO as a function of time (0–3 h). The electrode was held at −1.4 V vs. NHE during testing. The corresponding chronoamperometric curve for CuNPs/rGO is shown in inset. **b** Turnover frequency (TOF) as a function of the overpotential calculated for CuNPs/rGO (*black*) and Cu thin film (*red*). Inset is the evolution of the turnover from CuNPs on rGO measured over 24 h with an overpotential of 1.4 V. The *black arrow* indicates the change of the electrolyte solution. Calculations are based considering the total amount of copper and a 2-electron process (CO, CO_3^{2-} and $C_2O_4^{2-}$ products)

currents obtained from CuNPs on rGO electrodes immersed in CO_2-saturated solution compared to Ar-saturated solution, whereas rGO alone shows a limited catalytic activity (Figure S4). Furthermore, catalytic activity of CuNPs on rGO electrodes is significantly higher for ~70 nm-thick Cu film or CuNPs stabilized by polyallylamine (see Methods for details). Interestingly, a significant cathodic current was not observed using an electrode with passivated CuNPs with polyallylamine. Therefore, it can be stated that the presence of the polymer on the surface of CuNPs inhibits the copper activity. These results demonstrated the clear superior activity of the CuNPs supported on rGO nanosheets. Comparing the electrocatalytic activity of CuNPs on rGO and Cu thin film, it can be observed that higher current density can be achieved with lower overpotentials with rGO decorated

with CuNPs. For instance, at −1.2 V vs. NHE the current density observed in the CuNPs/rGO electrode is −0.24 mA cm^{-2}, while the same current density is reached at −1.54 V for Cu thin film. The current density obtained in the CuNPs/rGO at −1.54 V vs. NHE is −0.97 mA cm^{-2}, fourfold better than the Cu thin film.

Stability is an additional parameter in catalysis. To demonstrate the potential use of CuNPs on rGO for CO_2 reduction reaction, chronoamperometric measurements were carried out to investigate the stability (Fig. 4a). A constant overpotential of 1.4 V vs. NHE was applied on the CuNPs/rGO electrode for 3 h. Linear sweep voltammetry (LSV) was also performed with intervals of 1 h during the chronoamperometric measurements to check any overpotential shift. CuNPs on rGO exhibit stable current during the CO_2 reduction reaction (inset Fig. 4a). The improvement of the overpotential in the first hour under negative potential is likely due to the partial reduction of the oxide passivation layer on the copper nanoparticles as demonstrated by XPS and supported by Li et al. [17]. To gain insight into the reaction kinetics of the reduction process, we have calculated the turnover frequency (TOF) of the CuNP on rGO and Cu thin-film catalysts. The results of which are shown in Fig. 4b. It can be seen that the TOF obtained considering two-electron process (CO, CO_3^{2-} and $C_2O_4^{2-}$ products) is larger for CuNPs on rGO than the Cu thin films, suggesting that the CO_2 reduction is more favorable for CuNPs on rGO. It can also be seen from Fig. 4b that the number of turnovers increases linearly, indicating no substantial degradation of the activity of the Cu nanoparticles when deposited on rGO.

Conclusions

Our results suggest that rGO is a promising support for nanosized catalysts. The stabilization of Cu NPs on rGO not only improves the overall electrochemical stability but also enhances the catalytic activity for CO_2 reduction, in contrast with Cu NPs with polymer capping layer. Specifically, Cu nanoparticles on rGO have demonstrated lower overpotential and higher current density in comparison to pure Cu thin films and polymer capped Cu NPs. The enhanced stability may be attributed to partial covering of the NPs by a shell of rGO as observed in the TEM. Recent work proposes rough copper surface like nanoparticles as a way to enhance the selectivity towards hydrocarbons through uncoordinated copper sites [48]. These results suggest that rGO decorated with CuNPs may be a promising support for reducing CO_2.

Acknowledgments TA gratefully acknowledges the partial financial assistance provided by the US National Science Foundation (NSF) (Grant Nos: CAREER CHE-1004218, NSF DMR-0968937, NSF NanoEHS-1134289, NSF-ACIF for 2010, and NSF special creativity grant in 2011). DCBA and RS acknowledge the CAPES (Coordenação de Aperfeiçoamento de Pessoal de Nível Superior, Brazil) and the Fulbright Agency, USA for their fellowships and financial support for his graduate study.

References

1. Turner, J.A.: A realizable renewable energy future. Science **285**, 687–689 (1999)
2. Somorjai, G.A., Frei, H., Park, J.Y.: Advancing the frontiers in nanocatalysis, biointerfaces, and renewable energy conversion by innovations of surface techniques. J. Am. Chem. Soc. **131**, 16589–16605 (2009)
3. Silva, R., Asefa, T.: Noble metal-free oxidative electrocatalysts: polyaniline and Co(II)-polyaniline nanostructures hosted in nanoporous silica. Adv. Mater. **24**, 1878–1883 (2012). doi:10.1002/adma.201104126
4. Silva, R., Al-Sharab, J., Asefa, T.: Edge-Plane-Rich Nitrogen-Doped Carbon Nanoneedles and Efficient Metal-Free Electrocatalysts. Angew. Chemie. **124**, 7283–7287 (2012)
5. Gattrell, M., Gupta, N., Co, A.: A review of the aqueous electrochemical reduction of CO_2 to hydrocarbons at copper. J. Electroanal. Chem. **594**, 1–19 (2006)
6. Varghese, O.K., Paulose, M., Latempa, T.J., Grimes, C.A.: High-rate solar photocatalytic conversion of CO2 and water vapor to hydrocarbon fuels. Nano. Lett. **9**, 731–737 (2009)
7. Olah, G.A., Goeppert, A., Prakash, G.K.S.: Chemical recycling of carbon dioxide to methanol and dimethyl ether: from greenhouse gas to renewable, environmentally carbon neutral fuels and synthetic hydrocarbons. J. Org. Chem. **74**, 487–498 (2009)
8. Whipple, D.T., Kenis, P.J.A.: Prospects of CO_2 utilization via direct heterogeneous electrochemical reduction. J. Phys. Chem. Lett. **1**, 3451–3458 (2010)
9. Kuhl, K.P., Cave, E.R., Abram, D.N., Jaramillo, T.F.: New insights into the electrochemical reduction of carbon dioxide on metallic copper surfaces. Energy. Environ. Sci. **5**, 7050 (2012)
10. Centi, G., Perathoner, S.: Opportunities and prospects in the chemical recycling of carbon dioxide to fuels. Catal. Today **148**, 191–205 (2009)
11. Dewulf, D.W., Jin, T., Bard, A.J.: Electrochemical and surface studies of carbon-dioxide reduction to methane and ethylene at copper electrodes in aqueous-solutions. J. Electrochem. Soc. **136**, 1686–1691 (1989)
12. Hori, Y., Wakebe, H., Tsukamoto, T., Koga, O.: Electrocatalytic process of CO selectivity in electrochemical reduction of CO_2 at metal electrodes in aqueous media. Electrochim. Acta **39**, 1833–1839 (1994)
13. Azuma, M., Hashimoto, K.: Electrochemical reduction of carbon dioxide on various metal electrodes in low-temperature aqueous $KHCO_3$ media. J. Electrochem. Soc. **137**, 1772–1778 (1990)
14. Kaneco, S., Ueno, Y., Katsumata, H., Suzukib, T., Ohta, K.: Electrochemical reduction of CO_2 in copper particle-suspended methanol. Chem. Eng. J. **119**, 107–112 (2006)
15. Peterson, A.A., Abild-Pedersen, F., Studt, F., Rossmeisl, J., Norskov, J.L.: How copper catalyzes the electroreduction of carbon dioxide into hydrocarbon fuels. Energy. Environ. Sci. **3**, 1311 (2010)

16. Hori, Y., Murata, A., Takahashi, R.: Formation of hydrocarbons in the electrochemical reduction of carbon dioxide at a copper electrode in aqueous solution. J. Chem. Soc. Faraday. Trans. **1**(85), 2309 (1989)
17. Li, C.W., Kanan, M.W.: CO_2 reduction at low overpotential on Cu electrodes resulting from the reduction of thick Cu_2O films. J. Am. Chem. Soc. **134**, 7231–7234 (2012)
18. Xu, Z., Lai, E., Shao-Horn, Y., Hamad-Schifferli, K.: Compositional dependence of the stability of AuCu alloy nanoparticles. Chem. Commun. (Camb.) **48**, 5626–5628 (2012)
19. Perez, J., Gonzalez, E.R., Villullas, H.M.: Hydrogen evolution reaction on gold single-crystal electrodes in acid solutions. J. Phys. Chem. B. **102**, 10931–10935 (1998)
20. Eda, G., Chhowalla, M.: Chemically derived graphene oxide: towards large-area thin-film electronics and optoelectronics. Adv. Mater. **22**, 2392–2415 (2010)
21. Tang, L., Chang, H., Liu, Y., Li, J.: Duplex DNA/graphene oxide biointerface: from fundamental understanding to specific enzymatic effects. Adv. Funct. Mater. **22**, 3083–3088 (2012)
22. Liu, F., Song, S., Xue, D., Zhang, H.: Folded structured graphene paper for high performance electrode materials. Adv. Mater. **24**, 1089–1094 (2012)
23. Wu, Z.-S., Winter, A., Chen, L., Sun, Y., Turchanin, A., Feng, X., Müllen, K.: Three-dimensional nitrogen and boron co-doped graphene for high-performance all-solid-state supercapacitors. Adv. Mater. **24**, 5130–5135 (2012)
24. Wang, J., Zhang, X.-B., Wang, Z.-L., Wang, L.-M., Zhang, Y.: Rhodium–nickel nanoparticles grown on graphene as highly efficient catalyst for complete decomposition of hydrous hydrazine at room temperature for chemical hydrogen storage. Energy. Environ. Sci. **5**, 6885 (2012)
25. Li, Y., Wang, H., Xie, L., Liang, Y., Hong, G., Dai, H.: MoS2 nanoparticles grown on graphene: an advanced catalyst for the hydrogen evolution reaction. J. Am. Chem. Soc. **133**, 7296–7299 (2011)
26. Wu, Z., Yang, S., Sun, Y., Parvez, K., Feng, X., Müllen, K.: 3D nitrogen-doped graphene aerogel-supported Fe_3O_4 nanoparticles as efficient electrocatalysts for the oxygen reduction reaction. J. Am. Chem. Soc. **134**, 9082–9085 (2012)
27. Bagri, A., Mattevi, C., Acik, M., Chabal, Y.J., Chhowalla, M., Shenoy, V.B., Vivek, B.: Structural evolution during the reduction of chemically derived graphene oxide. Nat. Chem. **2**, 581–587 (2010)
28. Bagri, A., Grantab, R., Medhekar, N.V., Shenoy, V.B.: Stability and formation mechanisms of carbonyl- and hydroxyl-decorated holes in graphene oxide. J. Phys. Chem. C **114**, 12053–12061 (2010)
29. Dreyer, D.R., Park, S., Bielawski, C.W., Ruoff, R.S.: The chemistry of graphene oxide. Chem. Soc. Rev. **39**, 228–240 (2010)
30. Loh, K.P., Bao, Q., Eda, G., Chhowalla, M.: Graphene oxide as a chemically tunable platform for optical applications. Nat. Chem. **2**, 1015–1024 (2010)
31. Eda, G., Fanchini, G., Chhowalla, M.: Large-area ultrathin films of reduced graphene oxide as a transparent and flexible electronic material. Nat. Nanotechnol. **3**, 270–274 (2008)
32. Gómez-Navarro, C., Weitz, R.T., Bittner, A.M., Scolari, M., Mews, A., Burghard, M., Kern, K.: Electronic transport properties of individual chemically reduced graphene oxide sheets. Nano. Lett. **7**, 3499–3503 (2007)
33. Sahoo, N.G., Pan, Y., Li, L., Chan, S.H.: Graphene-based materials for energy conversion. Adv. Mater. **24**, 4203–4210 (2012)
34. Wen, Z., Cui, S., Pu, H., Mao, S., Yu, K.H., Feng, X.L., Chen, J.H.: Metal nitride/graphene nanohybrids: general synthesis and multifunctional titanium nitride/graphene electrocatalyst. Adv. Mater. **23**, 5445–5450 (2011)
35. Yu, X., Kuai, L., Geng, B.: CeO2/rGO/Pt sandwich nanostructure: rGO-enhanced electron transmission between metal oxide and metal nanoparticles for anodic methanol oxidation of direct methanol fuel cells. Nanoscale **4**, 5738–5743 (2012)
36. Li, Y., Zhou, W., Wang, H., Xie, L., Liang, Y., Wei, F., Idrobo, J.-C., Pennycook, S.J., Dai, H.: An oxygen reduction electrocatalyst based on carbon nanotube–graphene complexes. Nat. Nanotechnol. **7**, 394–400 (2012)
37. Hirata, M., Gotou, T., Horiuchi, S., Fujiwara, M., Ohba, M.: Thin-film particles of graphite oxide 1. Carbon. N. Y. **42**, 2929–2937 (2004)
38. Wang, Y., Asefa, T.: Poly(allylamine)-stabilized colloidal copper nanoparticles: synthesis, morphology, and their surface-enhanced Raman scattering properties. Langmuir **26**, 7469–7474 (2010)
39. Pedersen, D.B., Wang, S.: Surface plasmon resonance spectra of 2.8 ± 0.5 nm diameter copper nanoparticles in both near and far fields. J. Phys. Chem. C **111**, 17493–17499 (2007)
40. Goncalves, G., Marques, P.A.A.P., Granadeiro, C.M., Nogueira, H.I.S., Singh, M.K., Gracio, J.: Surface modification of graphene nanosheets with gold nanoparticles: the role of oxygen moieties at graphene surface on gold nucleation and growth. Chem. Mater. **21**, 4796–4802 (2009)
41. Acik, M., Lee, G., Mattevi, C., Pirkle, A., Wallace, R.M., Chhowalla, M., Cho, K., Chabal, Y.: The role of oxygen during thermal reduction of graphene oxide studied by infrared absorption spectroscopy. J. Phys. Chem. C **115**, 19761–19781 (2011)
42. Silva, R., Kunita, M.H., Girotto, E.M., Radovanovic, E., Muniz, E.C., Carvalho, G.M., Rubira, A.F.: Synthesis of Ag-PVA and Ag-PVA/PET-s20 composites by supercritical CO 2 method and study of silver nanoparticle. Growth. **19**, 1224–1229 (2008)
43. Kou, R., Shao, Y., Mei, D., Nie, Z., Wang, D., Wang, C., Viswanathan, V.V., Park, S., Aksay, I.A., Lin, Y., Wang, Y., Liu, J.: Stabilization of electrocatalytic metal nanoparticles at metal–metal oxide–graphene triple junction points. J. Am. Chem. Soc. **133**(8), 2541–2547 (2011)
44. Compton, O.C., Jain, B., Dikin, D.A., Abouimrane, A., Amine, K., Nguyen, S.T.: Chemically active reduced graphene oxide with tunable C/O ratios. ACS. Nano. **5**, 4380–4391 (2011)
45. Mattevi, C., Eda, G., Agnoli, S., Miller, S., Mkhoyan, K.A., Celik, O., Mastrogiovanni, D., Granozzi, G., Garfunkel, E., Chhowalla, M.: Evolution of electrical, chemical, and structural properties of transparent and conducting chemically derived graphene thin films. Adv. Funct. Mater. **19**, 2577–2583 (2009)
46. Hu, J., Liu, P., Chen, L.: Comparison of surface plasmon resonance responses to dry/wet air for Ag, Cu, and Au/SiO2. Appl. Opt. **51**, 1357–1360 (2012)
47. Blosi, M., Albonetti, S., Dondi, M., Martelli, C., Bald, G.: Microwave-assisted polyol synthesis of Cu nanoparticles. J. Nanoparticle. Res. **13**, 127–138 (2010)
48. Tang, W., Peterson, A.A., Varela, A.S., Jovanov, Z., Bech, L., Durand, W.J., Dahl, S., Norskov, J.K., Chorkendorff, I.: The importance of surface morphology in controlling the selectivity of polycrystalline copper for CO_2 electroreduction. Phys. Chem. Chem. Phys. **14**, 76–81 (2012)
49. Tomita, Y., Teruya, S., Koga, O., Hori, Y.: Electrochemical reduction of carbon dioxide at a platinum electrode in acetonitrile–water mixtures. J. Electrochem. Soc. **147**, 4164 (2000)
50. Amatore, C., Saveant, J.M.: Mechanism and kinetic characteristics of the electrochemical reduction of carbon dioxide in media of low proton availability. J. Am. Chem. Soc. **103**, 5021–5023 (1981)
51. Calderón, C.A., Ojeda, C., Macagno, V.A., Paredes-Olivera, P., Patrito, E.M.: Interaction of oxidized copper surfaces with alkanethiols in organic and aqueous solvents. the mechanism of Cu_2O reduction. J. Phys. Chem. C **114**, 3945–3957 (2010)